191 (2024) 206944

Contents lists available at ScienceDirect

Applied Catalysis O: Open

journal homepage: www.elsevier.com/locate/apcato

Next-generation photocatalytic system: Ga_2O_3-modified Ga Nanoislands on graphene for H_2 production

Miroslav Bartošík [a,b,c,*], Miroslava Filip Edelmannová [d], Jindřich Mach [a,b], Kamila Kočí [c,d,*]

[a] Central European Institute of Technology (CEITEC), Brno University of Technology (BUT), Purkyňova 656/123, 612 00 Brno, Czech Republic
[b] Institute of Physical Engineering, Brno University of Technology, Technická 2, Brno 616 69, Czech Republic
[c] Department of Physics and Materials Engineering, Faculty of Technology, Tomas Bata University in Zlín, Vavrečkova 275, Czech Republic
[d] Institute of Environmental Technology, CEET, VSB-Technical University of Ostrava, 17. listopadu 2172/15, Ostrava-Poruba 708 00, Czech Republic

ARTICLE INFO

Keywords:
Photocatalysis
Hydrogen generation
Ga material
Water splitting

ABSTRACT

Study investigates Ga_2O_3/Ga on Graphene/SiO_2/Si, prepared via temperature-controlled growth of Ga, for photocatalytic hydrogen generation, marking the first exploration of this system for such purpose. Thin surface ultra-wide band gap Ga_2O_3 layer effectively photoemits electron-hole pairs under UVC and the metallic Ga cores enhance electric field separating charge carriers by formation of localized surface plasmon (LSP) resonances. These effects increase hydrogen yields. Computational analysis of LSP-induced electric field enhancement quantitatively supports proposed fundamental mechanism underlying sample's photoactivity. The most active photocatalyst (Ga-M) with medium-size Ga particles (radius 14 nm) exhibited ten thousand times higher activity per gram than commercial TiO_2.

1. Introduction

Unfortunately, global industrial development is having an impact on the environment by increasing contaminants in natural ecosystems. This situation could be improved both by addressing the reduction of contaminants already present in the environment and by preventing pollution through renewable energy sources (wind, geothermal, solar, etc.) [1,2].

Recently, attention has been focused on hydrogen energy because of its many advantages, namely storage, transportability, cleanliness, higher calorific value than natural gas and zero emissions. Photocatalytic water splitting can be a promising green process for hydrogen production because it uses solar energy and water resources to produce hydrogen and oxygen. One of the main factors influencing photocatalytic water splitting is electron-hole recombination, which can be reduced by using so-called sacrificial reagents such as methanol, ethanol, glycerol, ethylene glycol, etc. [2–4].

TiO_2 is the best known and most widely used photocatalyst to date, but its real applications are limited due to its ability to absorb UV radiation (4–5% of solar radiation) and the rapid recombination of electron-hole pairs. So, either TiO_2 is modified or other materials are sought that would have higher photocatalytic activity in the visible region [1].

The formation of composite material can improve the selective electrostatic adsorption effect and the separation efficiency of photogenerated photocatalyst carriers, which will promote the surface reaction and greatly enhance the efficiency. Metallosilicate materials are important structured solids with favorable physicochemical properties, i.e. good conductivity, large pore volume, high specific surface area, excellent colloidal stability and rich surface chemistry. In addition, SiO_2 is an economically viable material, it can be obtained from agricultural wastes such as rice straw (hydrated $SiO_2 \sim 15\%$). SiO_2-based materials allow selective isomorphic substitution of silicon by various elements (for example, the insertion of trivalent Ga^{3+} cations) [1,5–9].

Graphene also exhibits remarkable properties for photocatalysis applications; it has a high specific surface area, high electron mobility. Efficient doping of graphene can be achieved using metals that allow controlled modification of the Fermi energy throughout the system. Nanocomposites of graphene-metal are promising materials used in plasmonic-enhanced photonics, advanced plasma graphene-based photodetectors, sensors (Pt/graphene/SiC) and photocatalysis (Ag-graphene-based nanocomposites.

Gallium is a non-noble metal with a melting point slightly below 30 °C, it exhibits subcooling behavior and thus provides high stability to

* Corresponding author at: Department of Physics and Materials Engineering, Faculty of Technology, Tomas Bata University in Zlín, Vavrečkova 275, Czech Republic.
E-mail addresses: bartosik@fme.vutbr.cz (M. Bartošík), kamila.koci@vsb.cz (K. Kočí).

https://doi.org/10.1016/j.apcato.2024.206944
Received 31 January 2024; Received in revised form 9 April 2024; Accepted 23 May 2024
Available online 24 May 2024

the liquid droplets. Ga droplets have high surface tension and tend to self-organize into densely packed two-dimensional arrays, which should result in homogeneous growth of high-density nanoparticles over large areas of the substrate [10,11]. In addition, Ga is a shallow acceptor (27 meV) in Si from an electrical point of view and is therefore compatible with applications in silicon devices [12–19]. Moreover, the gallium is a promising material for plasmonics having a Drude-like dielectric function with a bulk plasma frequency 14 eV. It enables the excitation of coherent oscillations of electrons on Ga surface, called a localized surface plasmons (LSP) within the broad bandwidth over which gallium is metallic from the ultraviolet through the visible into the infrared wavelengths in which the gallium is metallic [20].

It has been found, the gallium nanoparticles exposed to atmospheric conditions are oxidized on its surface. Such a gallium oxide (Ga_2O_3) cover layer has a thickness of approximately 1 nm independent of the gallium nanoparticle dimensions [21]. The native oxide shell protects the pure metallic Ga core providing both structural and chemical stability over many years. Ga_2O_3 is a semiconductor with an ultra-wide band gap of 4.8 eV, a high theoretical breakdown field (8 MV/cm), and a high thermal stability and conductivity from 0.1 to 0.3 W/(cm·K). Therefore, it has been attracting considerable attention for applications in solar-blind UV (200–280 nm) photodetectors, solar-cells, and high-power electronics [22].

Here we report the synthesis of graphene-coated Si/SiO_2 wafers with gallium droplets covered by a thin native Ga_2O_3 shell in an ambient atmosphere. The gallium on graphene showed island-like growth, and the size of the Ga islands was controlled by the deposition temperature used, so the higher the temperature, the larger the islands formed. These materials were tested in hydrogen generation using methanol as an electron donor. Our samples show impressive hydrogen production under UV irradiation in comparison with TiO_2. The behavior is being explained by the electron-hole pair formation in Ga_2O_3 cover assisted by electric field enhancement due to the formation of localized surface plasmon (LSP) resonances in the Ga island cores which is also supported by the finite element method (FEM) based on the stationary solution of Maxwell's equation for studied samples. Moreover, it should be noted that the prepared samples in the form of thin wafers with an active layer can be easily separated from the aqueous solution, which is a great advantage compared to powder photocatalysts. The findings open a new perspective toward new materials for hydrogen production.

2. Experimental part

2.1. Preparation of samples

The samples are composed from Si/SiO_2 wafer covered by graphene with gallium droplets. The fabrication procedure is following. Single-domain graphene flakes were grown by a standard low-pressure chemical vapor (CVD) method on a Cu substrate acting as a catalyst. Graphene was grown in home-made chamber following the three-step procedure: (1) pumping down to a base pressure of 10^{-3} Pa, (2) filling with hydrogen at a flow of 4 sccm at pressure 10 Pa and annealing at 1000 °C, and (3) introducing the H_2/CH_4 mixture for 30 min at a flow of 40 sccm and total pressure 70 Pa to initiate graphene growth. Subsequently, the graphene was transferred onto Si/SiO_2 wafers by wet transfer method (Si/SiO_2/graphene layer order). The original silicon dioxide wafers are composed of nonconductive thermally grown SiO_2 (280 nm) layer covering a p-doped Si(100) substrates (resistivity of 1.5×10^{-3} Ωcm, provided by the ON semiconductor).

All the Ga depositions were performed on graphene site of as prepared substrates. The samples were loaded into an ultrahigh vacuum (UHV) chamber with a pressure of 10^{-8} Pa and annealed at 300 °C for 24 h to clean the surface prior to Ga deposition. Ga atoms of thermal energy were evaporated using a home-made effusion cell composed from pyrolytic boron nitride boat inside a Mo crucible heated at Ga evaporation temperature. The total mass of Ga atoms deposited onto the surface was kept constant 2 μg and took 180 min. The depositions were carried out at different substrates temperatures: 25 (RT), 200, and 300 °C, corresponding the marking of samples Ga—S, Ga-M, and Ga-L, respectively.

2.2. Photocatalytic experiments

The photocatalytic experiments were performed in a batch stainless steel photoreactor. The solid photocatalyst (Si/SiO_2 wafers with graphene and gallium) was in 100 ml of 50% methanol. Before starting the photocatalytic reaction, the photoreactor was tightly closed and saturated with helium at a pressure of 125–130 kPa for 30 min. The pressure of the gas phase in the photoreactor was continuously monitored during the reaction and during batch preparation prior to starting the reaction. The suspension was illuminated by an UVC 8 W Hg lamp ($\lambda_{max} = 254$ nm, Ultra-Violet Products Inc., USA) situated in the horizontal position on top of the quartz glass window of the photoreactor. The photocatalytic reactions were initiated by turning on the UVC lamp. Gaseous samples were taken in certain time intervals by a gas-tight syringe through a septum and then immediately analyzed on a gas chromatograph (Shimadzu Tracera GC-2010) equipped with a barrier ionization discharge (BID) detector. The photocatalytic tests were repeated to confirm the reproducibility of the experiments and stability of investigated samples.

3. Results

3.1. In-situ lateral characterization of Ga nanostructures by UHV SEM

During the deposition of gallium, the sample surface was in-situ monitored by UHV SEM microscope (producer TESCAN ORSAY). The gallium atoms diffuse along the graphene surface and form islands of nanometer dimensions as can be seen in Fig. 1. Although the mass of deposited gallium was constant (2 μg), it is obvious the dimensions of circular islands increased with the substrate temperature. This is caused by an enhanced surface diffusion length of gallium atoms. Size analysis of the Ga islands shown in Fig. 1 using a generalized Hough transform fitting each island with a circle proved the gaussian distribution of radii, and the results are summarized in Table 1. Increasing substrate temperature from 25 °C to 200 °C resulted in a 40% larger island radius (10 nm ➔ 14 nm), and additional heating from 200 °C to 300 °C caused a 70% growth (14 nm ➔ 24 nm). On the other hand, the higher temperature strongly reduced the number of Ga nano-islands present in SEM images (Fig. 1, Table 1).

3.2. Ex-situ height-profile characterization of Ga nanostructures by AFM

Since SEM secondary electron intensity images do not provide precise information about the height of Ga islands, the surface topography was imaged by atomic force microscopy (AFM) under atmospheric conditions. Fig. 2 shows the AFM topography of Ga islands at RT. The Ga islands formed spherical caps of nanometer dimensions with a height slightly lower than the radius. The more careful analysis determined the radius-to-height ratio from 61% to 90%. Based on the previous assumptions and the knowledge of Ga radii from SEM analysis, the volume and surface of deposited gallium can be compared (Table 2). It must be noted the Ga nano-islands observed using ambient AFM have already been covered by a Ga_2O_3 shell with a thickness of 1 nm.

The surface area comparison proved a rapid growth of Ga_2O_3/Ga surface of islands with lower substrate temperature and smaller islands. Such behavior is typical for nanostructures, although an almost three-times (2.8 x) larger surface for room temperature, and an almost two-times (1.8 x) larger surface at 200 °C relative to the value valid for 300 °C is a relatively high increase. On the other hand, the bulk volume analysis (Table 2) proved a slight relative difference in the model-based estimation of volume (< 10%), which agrees with the mass of deposited

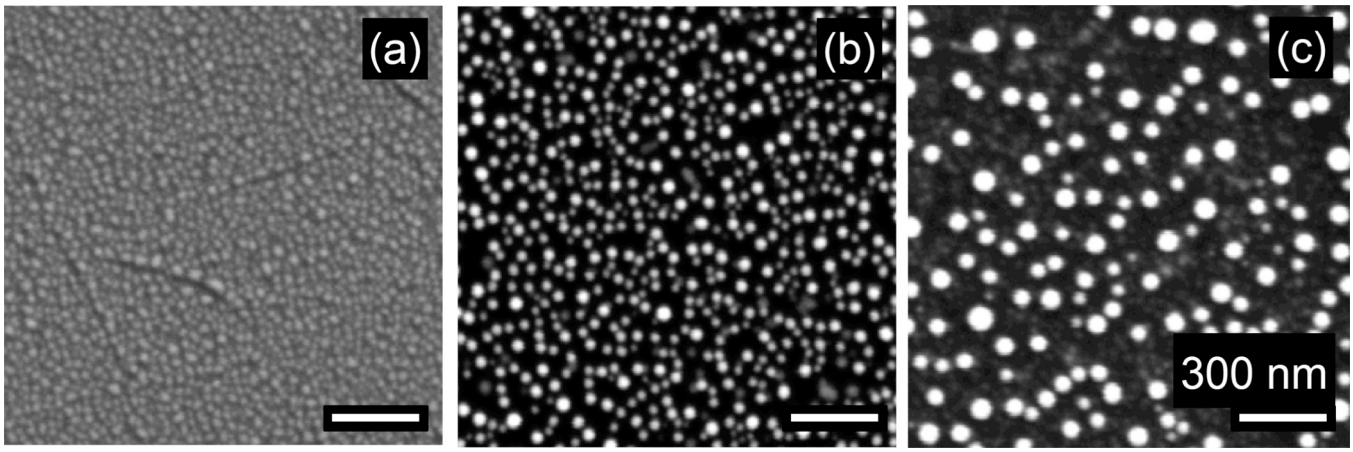

Fig. 1. In-situ UHV scanning electron microscopy image of Ga islands deposited on SiO_2 surface at RT (a), 200 °C (b) and 300 °C (c). The area of each image is 1.5 × 1.5 μm^2. The dimension of horizontal white scale bar is 300 nm.

Table 1
The summary of Hough's transform results of Ga islands shown in Fig. 1.

Marking of sample	Substrate temperature	Number of islands	Average radius
Ga-S	25 °C (RT)	3027	10 ± 2 nm
Ga-M	200 °C	1018	14 ± 4 nm
Ga-L	300 °C	166	24 ± 7 nm

gallium was constant. Slight discrepancies can be attributed to the model assumptions and the analyzing only a small area (1.5 × 1.5 μm^2) compared to a whole sample surface (1 × 1 cm^2).

3.3. XPS analysis

After the Ga deposition and exposure of samples to the ambient air (before photocatalytic tests), the X-ray photoelectron spectroscopy (XPS) was measured using a commercial instrument Omicron DAR400 X-ray source and EA125 electron spectrometer. The XPS spectra of samples show three main peaks: Ga $2p_{3/2}$, O 1 s, and C 1 s as can be seen in a typical measurement of the Ga—S sample depicted in Fig. 3. The Ga $2p_{3/2}$ peak is a characteristic peak for Ga metal, and the shift in its binding energy provides information about oxidation. The O 1 s peak indicates the presence of oxygen, and can be attributed to silicon dioxide, environmental oxygen atoms, and partly also to gallium oxide (see below next paragraph). The C 1 s peak is associated with the graphene substrate.

Decomposing the Ga peak (Ga $2p_{3/2}$) into the Ga—O and Ga—Ga contributions offers further insight (Fig. 3 - detail). The Ga—O peak arises from the bonding of gallium oxygen atoms, such as in gallium oxide (Ga_2O_3) or other Ga—O species. The Ga—Ga peak, on the other hand, arises from the bonding of gallium atoms with each other, such as in metallic gallium or gallium nanoparticles. The relative intensities of the Ga—O and Ga—Ga peaks provide information about the relative abundance of these two types of bonds in the sample. The spectrum shown in Fig. 3 has a relatively high Ga—O contribution. The reason is the Ga—S sample grown at room temperature has the smallest gallium nanoparticles (Fig. 1 a and Table 1) and the ambient surface oxidation thickness remains constant at 1 nm as has been proved [21]. The Ga—O peak would be partially suppressed at the expense of Ga—Ga in case of higher temperature deposited samples with larger nanoparticles (Ga-M, Ga-L). However, as a surface-sensitive technique with an effective depth

Table 2
The volume and surface area of nano-islands imaged by SEM in Fig. 2 assuming a spherical-cap shapes and the radius-to-height ratios derived from an AFM analysis. The volume and surfaces expressed relatively to values obtained at substrate temperature 300 °C.

Marking of sample	Substrate temperature	V (V at 300 °C)	S (S at 300 °C) S/S_{300}
Ga-S	25 °C (RT)	1.09	2.8
Ga-M	200 °C	1.08	1.8
Ga-L	300 °C	1	1

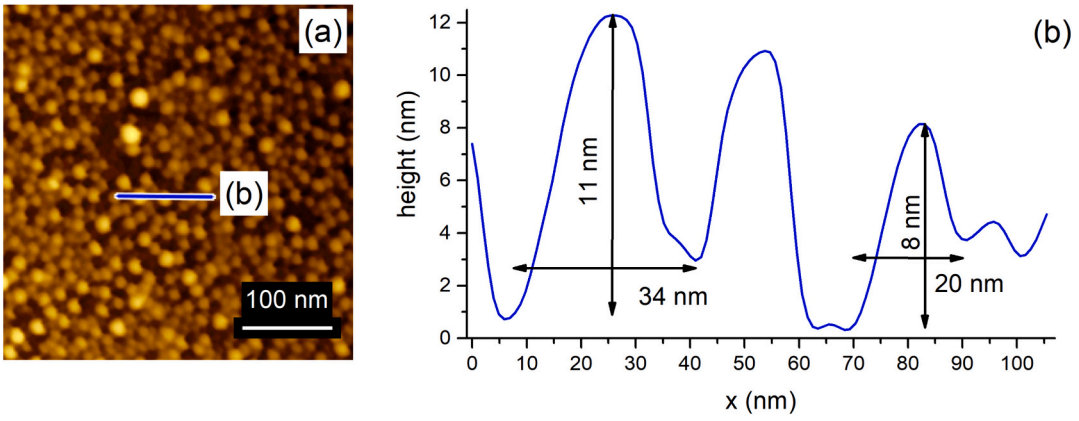

Fig. 2. (a) Ex-situ atomic force microscopy topography image of Ga islands deposited on SiO_2 surface at RT. (b) Height profile in cross-section along the blue solid horizontal line highlighted in (a). (For interpretation of the references to colour in this figure legend, the reader is referred to the web version of this article.)

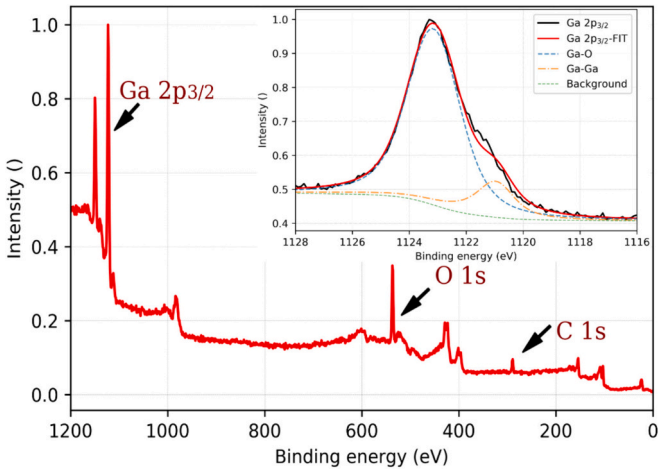

Fig. 3. XPS spectrum of Ga_2O_3/Ga nanostructures grown on graphene/Si/SiO_2 surface at room temperature (Ga—S sample). The shift of gallium peak (Ga $2p_{3/2}$) caused by surface oxidation of Ga nanoparticles after atmosphere exposure is in detail.

of information of approximately 3 nm, the XPS cannot map effectively the amount of Ga in the cores of larger gallium clusters and as a result, the suppression is not that significant.

3.4. Photocatalytic hydrogen generation from methanol/water solution

The photocatalytic generation of hydrogen from methanol/water solution could be described by the overall Eq. [23]:

$$CH_3OH(l) + H_2O(l) \xrightarrow{hv,TiO_2} 3H_2(g) + CO_2(g) \quad (1)$$

During this reaction, gaseous H_2 is produced, involving the half-reaction of oxidation:

$$CH_3OH(l) + H_2O(l) + 6\,h^+ \xrightarrow{hv,TiO_2} 6\,H^+ + CO_2(g) \quad (2)$$

followed by reduction:

$$6\,H^+ + 6\,e^- \rightarrow 3\,H_2 \quad (3)$$

As shown in Fig. 4 (a) and (b), the Ga samples show a relatively comparable photocatalytic activity. Specifically, two samples Ga—S and Ga-L exhibits from 6159 to 6531 hydrogen production which is below commercial TiO_2 – P25 with 7339 ppm after 4 h of UVC irradiation (λ_{max} = 254 nm). On the other hand, the Ga-M sample hydrogen production 8218 ppm is above all other samples.

The situation is completely different when the photocatalytic activity per unit mass of an active material is compared. Although an individual Ga_2O_3/Ga/Graphene/SiO_2/Si sample mass is 70 mg, each sample contains only about 2 μg of an active Ga_2O_3/Ga/Graphene material, while the amount of TiO_2-P25 was 100 mg). It implies the yields for Ga materials and TiO_2 shown in Fig. 4 are comparable, nevertheless, the amount of an active ingredient in the case of Ga materials is many orders of magnitude lower (100 mg / 2 mg = $50{\cdot}10^3$). The hydrogen yields expressed in μmol per g of active catalysts prove the investigated Ga samples are more than ten thousand times (10^4) more active than the commercial TiO_2-P25, as shown in Fig. 5 (hydrogen yields of TiO_2-P25 were multiplied ten-thousand times for better recognition).

At the end of this section, it should be also noted that the samples of Ga_2O_3/Ga/Graphene/SiO_2/Si were also exposed to UVA irradiation (λ_{max} = 365 nm), however, there was no photocatalytic activity at this wavelength.

4. Calculations of electric field enhancement close to gallium nanostructures

Based on the fact the photocatalytic reaction of studied samples occurred when irradiated with an UVC (λ_{max} = 254 nm) lamp corresponding the energy of 4.8 eV, and not when exposed to UVA irradiation (λ_{max} = 365 nm) with energy of 3.4 eV, the main active material is a thin Ga_2O_3 layer covering Ga islands. The reason is the Ga_2O_3 is a semiconductor with an ultra-wide band gap of 4.8 eV effectively blocking the creation of electron-hole pairs for UVA and, conversely, allowing the formation of pairs for UVC.

Therefore, the higher amount of gallium oxide could lead to higher hydrogen production. Since the gallium oxide is involved only on a gallium surface, the samples with a larger surface area corresponding to smaller gallium islands should be significantly more active. For example, if the surface area of the smallest gallium islands (Ga—S) is 2.8 times larger than the surface area of the largest ones (Ga-L, Table 2), a similar increase of hydrogen production could be expected. However, both of this samples produces a similar amount of hydrogen (Fig. 5). The explanation of such behavior could be found in an enhancement of electric field caused by the existence of localized surface plasmon (LSP) resonances in metallic gallium cores. Such an electric field enhancement is higher for larger metallic particles. E. g., for a metallic spherical particle of radius r with a frequency dependent dielectric function

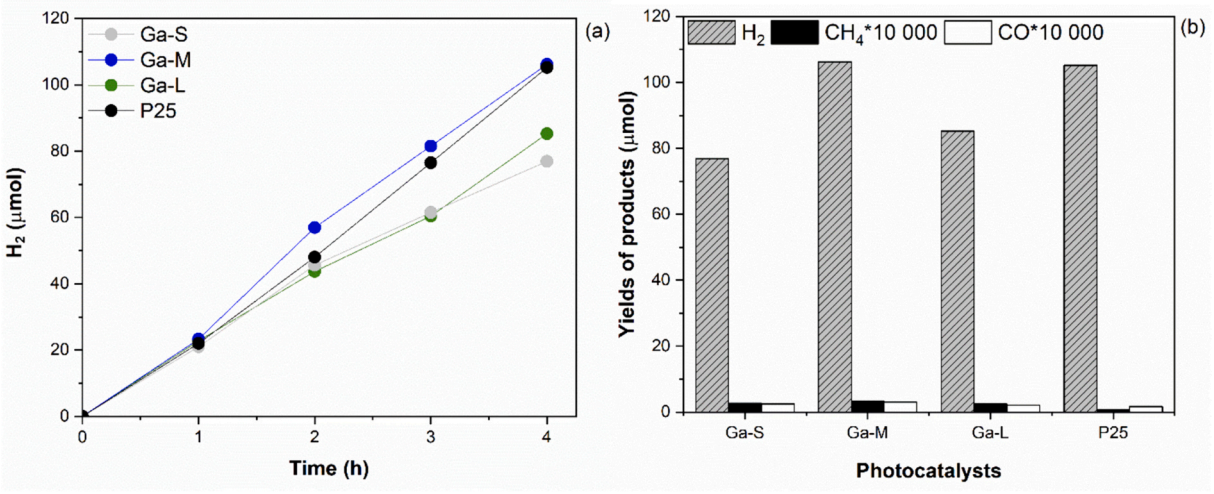

Fig. 4. (a) Time dependence of hydrogen yields (in μmol) during the photocatalytic decomposition of the methanol-water mixture over Ga materials and P25 at irradiation of 254 nm and (b) yields of all products after 4 h of irradiation (λ_{max} = 254 nm) over Ga materials and commercial TiO_2 - P25.

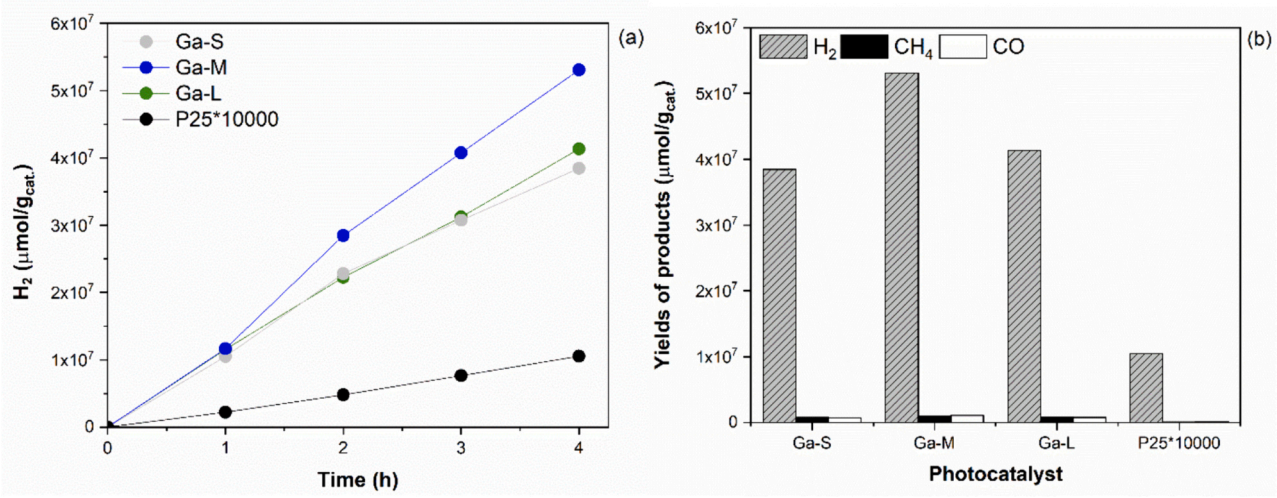

Fig. 5. (a) Time dependence of yields of hydrogen (in μmol/$g_{cat.}$) during the photocatalytic decomposition of the methanol-water mixture in the presence of investigated photocatalysts and P25 and (b) yields of all products after 4 h of irradiation ($\lambda_{max} = 254$ nm) over Ga materials and commercial TiO_2 - P25 in μmol/$g_{cat.}$.

$\varepsilon(\omega)$ surrounded by a dielectric material with relative permittivity ε_r, the enhancement of an outside electric field is given by the polarizability [24]:

$$\alpha = 4\pi r^3 \frac{\varepsilon(\omega) - \varepsilon_r}{\varepsilon(\omega) + 2\varepsilon_r}. \quad (4)$$

The eq. (4) indicates, the extreme LSP induced electric field enhancement for a negative metallic dielectric function $\varepsilon(\omega) \rightarrow -2\varepsilon_r$. By applying a simple non-damped free-electron Drude-Lorentz model of dielectric function dependency of metal in form [25]:

$$\varepsilon(\omega) = 1 - \frac{\omega_p^2}{\omega^2}, \quad (5)$$

where the ω_p is a plasma frequency, for gallium core $\omega_p = 2 \bullet 10^{16}$ Hz (14 eV [20]), the wavelengths of radiation leading to LSP resonances can be estimated. The analytical formula (4) gives a relatively good insight into the mechanism of LSP induced field enhancement, however, it is limited only on spherical metallic particles surrounded by a simple dielectric characterized by the ε_r. Since the gallium islands in experiments have half-spherical shapes, and they are surrounded by a complex environment composed of Ga_2O_3 ($\varepsilon_r = 10$), graphene (semi-metal), water ($\varepsilon_r = 81$), and methanol ($\varepsilon_r = 33$), the numerical calculations solving the Maxwell's equations using COMSOL Multiphysics® software [26] were performed.

The calculated electric potential and intensity enhancement for a gallium half-sphere with radius of 24 nm corresponding to the average radius of Ga-L sample is depicted in Fig. 6. The computation was performed as stationary. The impact of incident wavelength was considered indirectly using optimization of gallium dielectric function (eq. 2) so that the electric field would be maximally enhanced. Such a maximum occurred for $\varepsilon(\omega) = -56.9$ corresponding the wavelength 669 nm. Comparing this value with the LSP resonance condition of a spherical-particle $\varepsilon(\omega) \rightarrow -2\varepsilon_r$ (derived from eq. 1), it is obvious the value is not directly related to the relative permittivity of surrounding Ga_2O_3 cover or water-methanol mixture, however, it is close to the mean valuer for methanol ($-2\varepsilon_r = -66$). The calculation shows the formation of dipole with an opposite orientation to the external field (Fig. 6 a). The highest electric potential enhancement value 3.68 is localized on the interface of gallium core surface and its oxide cover. The maximum electric intensity enhancement value 215 ($\approx e^{5.37}$) of electric intensity is even more extreme and sharply focused into the Ga_2O_3 cover (Fig. 6 (b) – scaled in natural logarithm to improve the visibility).

The horizontal cross-sections through the maps of electric potential and intensity enhancement at the points of their maxima (approximately at the center of the gallium half-sphere height) for three different gallium radii 10, 14, and 24 nm (corresponding the average Ga radius in measured samples) are depicted in Fig. 7. It is evident, the larger gallium core results in stronger electric field enhancement. Although the potential enhancement for the smallest radius is only 1.04, the corresponding electric field gain achieves a significant value of 61. For larger Ga islands, the gains are even higher. As explained in the previous paragraph, optimized dielectric values of the Ga core were found. For

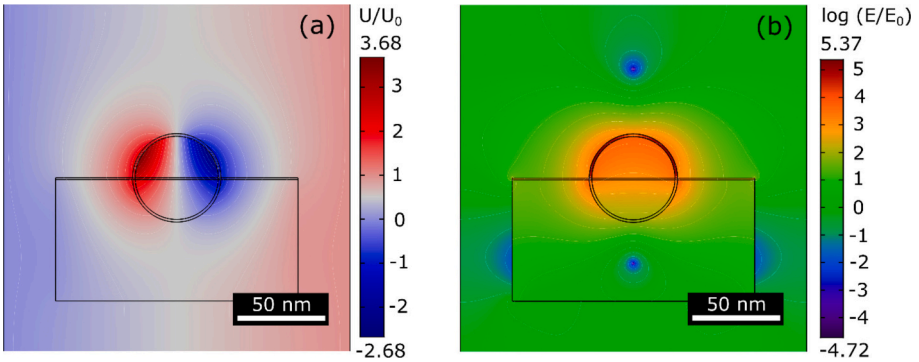

Fig. 6. The computation of a calculated (a) electric potential and (b) intensity enhancement in close proximity of Ga half-sphere with radius of 24 nm, covered by a thin 1 nm Ga_2O_3 layer placed on graphite (1 nm) / SiO_2 (70 nm) substrate. The result for an optimized maximum gain corresponding to an illumination by a wavelength of 669 nm (red). (For interpretation of the references to colour in this figure legend, the reader is referred to the web version of this article.)

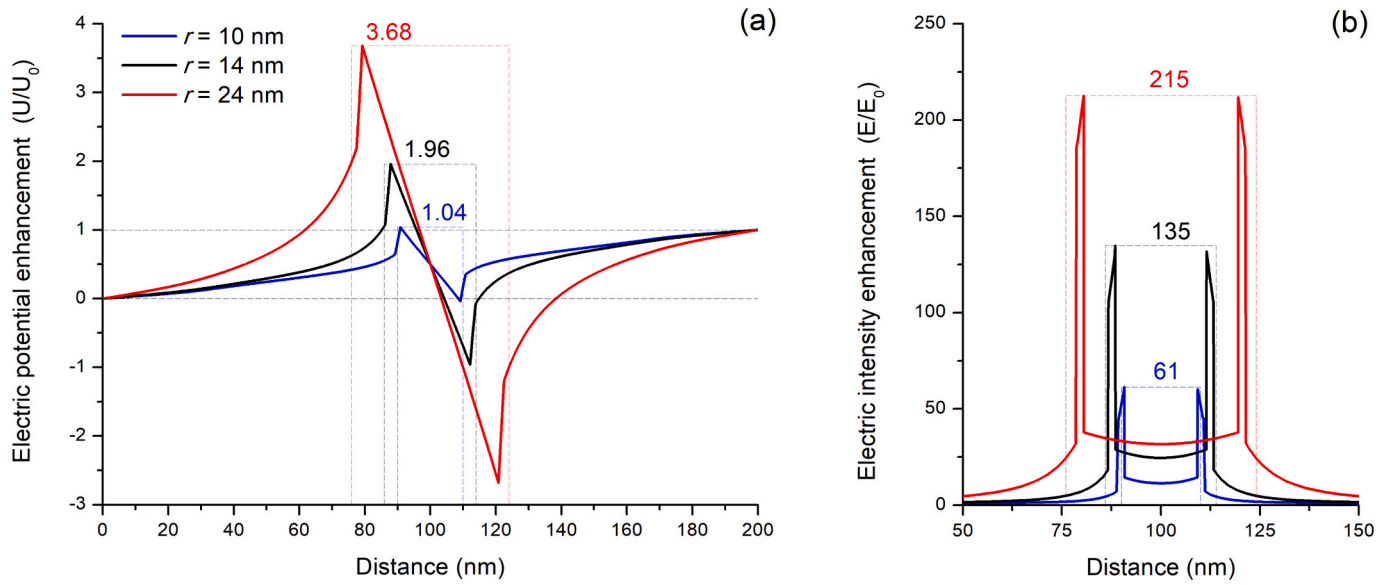

Fig. 7. The horizontal cross-section of a calculated (a) electric potential and (b) intensity enhancement through the gallium half-sphere at the point of a maximum value for radii 10, 14, and 24 nm corresponding average sizes of Ga islands deposited at RT, 200 °C, and 300 °C (see above Fig. 6). The vertical lines of dashed rectangles indicate the dimensions of half-spheres, and the vertical lines determine the maximum of enhancement.

the gallium half-spheres with radii 10, and 14 nm, the maximally enhancing dielectric function values were − 46.9, and − 43.5 corresponding to the wavelengths 587 nm, and 609 nm, respectively.

The computations prove a strong enhancement of electric field at the edges of a gallium core by the formation of localized surface plasmons (LSP). Such a field can contribute to a more effective separation of electron and holes previously created in the Ga_2O_3 cover under UV radiation exposure and consequently increase a photocatalytic activity. Although the plasmonic resonances occur for wavelength in visible range, the way the experiment was performed did not exclude the presence of visible daylight. Due to its low energy, the visible light completely propagates through the ultra-wide band gap oxide cover, and creates the LSP resonances of metallic core. Moreover, the simulations show the enhancement is stronger for larger gallium islands

5. Discussion

Photocatalytic activity can be influenced by many factors, e.g. specific surface, particle size, band gap, different cocatalysts, lifetime of generated electron-hole pairs etc. The experimental and computational results indicate two key factors determining the extremely enhanced photocatalytic activity of Ga_2O_3/Ga/Graphene/SiO_2/Si samples. The first one is a Ga_2O_3 cover layer responsible for the creation of electron-hole pairs. The second one is a formation of localized surface plasmons (LSP) in Ga cores strongly enhancing the electric field under illumination as can be seen in Fig. 8.

Unlike the bulk Ga_2O_3 materials studied by other groups [22,27–31], the investigated samples contain a gallium oxide as a thin layer on gallium particle surface suppressing the bulk recombination. Hence the incident electromagnetic ultra-violet wave energy is effectively used to create electron-hole pairs on the surface close to the water-methanol mixture ensuring significant hydrogen production. Moreover, the effect is multiplied by the LSP resonances of gallium cores utilizing the rest of electromagnetic radiation energy in the visible range, when the enhancement of the field separates electrons and holes restraining their recombination and gaining hydrogen production. These factors together with the effective charge transfer between individual gallium islands mediated by the underlying graphene significantly increase yields per gram in comparison with commercial TiO_2 samples.

Both of these effects: electron-hole pair creation in the Ga_2O_3 cover

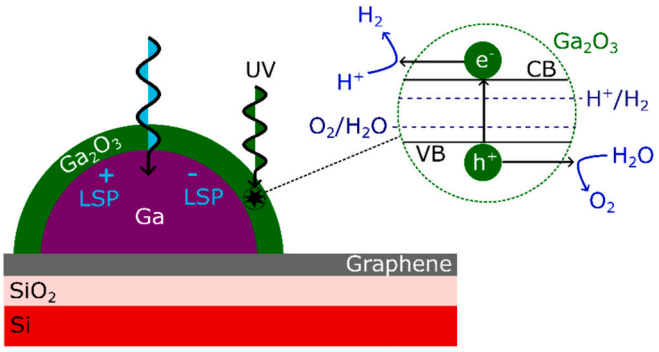

Fig. 8. The schematic of fundamental principles behind photocatalytic H_2 production from decomposition of methanol-water mixture over Ga_2O_3/Ga nanostructures on graphene/Si/SiO_2 surface.

layer and electric field enhancement by LSP resonances increasing the hydrogen yield have the opposite dependency on the size or radius of gallium islands. While the amount of generated electron-hole pairs increases with the surface area containing Ga_2O_3, which is higher for the Ga islands having a lower radius (Table 2, 4th column), the enhancement of electric field caused by LSP resonances increases with the Ga island radii (Fig. 7 (b)). It can be used to explain the dependency of hydrogen yield as a function of the Ga island radius (Fig. 9). The hydrogen yields are similar for the smallest and largest Ga islands deposited at substrate temperatures 25 °C and 300 °C. The reason is the smallest islands (25 °C) have the highest electron-hole pair production and maximally suppressed the LSP-induced field gain, contrary, the largest islands (300 °C) have the strongest LSP enhancement and the lowest electron-hole pair contribution. As a result, the hydrogen production is approximately the same. The maximum hydrogen yield exhibits samples with the medium Ga island sizes grown at a temperature of 200 °C where both the effects optimally contribute to hydrogen production. Such a trend is also obvious by comparing the product of the Ga surface increase (Table 2, 4th column) multiplied by calculated electric field enhancement (Fig. 7 (b)) for typical radii (Fig. 9, red squares). Assuming the plasmon enhancement is proportional to specific surface volume ($SSV = \frac{4}{3}\pi r^3/4\pi r^2 \sim r$ for a spherical particle)

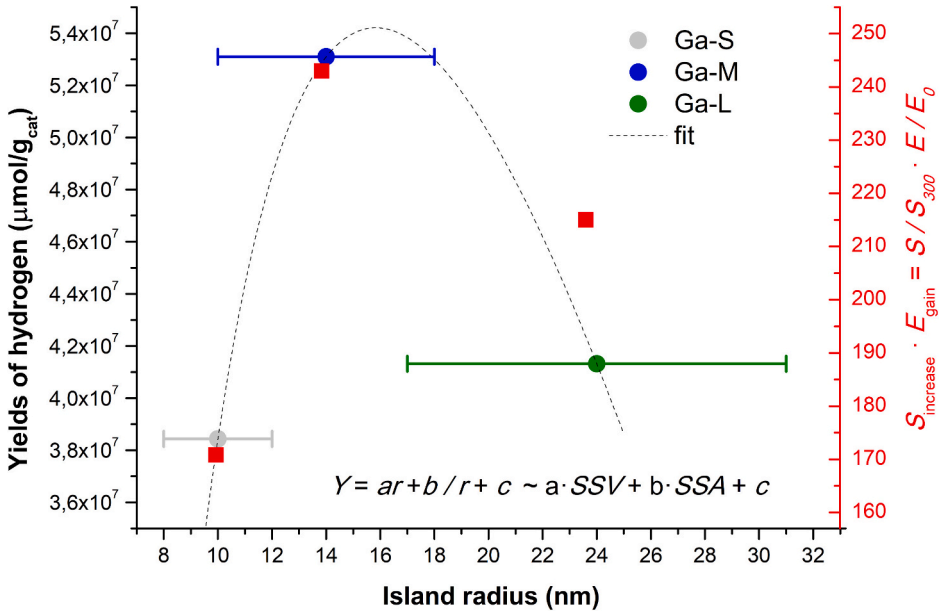

Fig. 9. The yields of hydrogen per gram as a function of Ga_2O_3/Ga island radius fitted by a curve considering the plasmon effect proportional to specific surface volume (*SSV*) and electron-hole pair production growing with the specific surface area (*SSA*). The red squares scaled on the right axis correspond to the product of the measured surface increase multiplied by the calculated LSP-induced electric field enhancement ($S_{increase} \bullet E_{gain}$) that strongly correlates with the real hydrogen yield. (For interpretation of the references to colour in this figure legend, the reader is referred to the web version of this article.)

determining the ratio of gallium particle to its surface, and the electron-hole pair generation proportional to specific surface area ($SSA \sim r^{-1}$), the experimentally measured yields can be fitted by a suitable curve describing these fundamental principles (Fig. 9 – dotted black curve). Here, the specific surfaces (*SS*) are used instead of surface or volume, since at a constant amount of the deposited Ga material, the surface of particles grows on behalf of volume and vice versa.

The impact of particle size on photocatalytic hydrogen generation in the presence of Ga_2O_3/Ga/Graphene/SiO_2/Si samples has not been studied so far. However, the optimum particle size corresponding to the highest yields in other photocatalytic reactions has been found e.g. the photocatalytic reduction of CO_2 in presence of TiO_2 (with an optimal size of 14 nm) [32] or presence of gold/titanium oxide/calcium carbonate photocatalysts (with an optimal size of 12 nm) [33] or degradation of 1,1-diphenyl-2-picrylhydrazyl (DPPH) on presence of ZnO and CeO_2 nanoparticles (with an optimal particle size 33 and 30 nm, respectively) [34].

In general, the particles of larger sizes exhibit higher stability in time, even though they are less photoactive. On the other hand, the smaller particle size exhibit higher photoactivities. However, ultra-fine particles (in our case smaller than 28 nm, i.e. radius = 14 nm) also have certain disadvantages [35]. When the particle size decreases, the density of recombination centers increases and thus the surface electron-hole recombination increases. Ultrafine particles (in our case 20 nm i.e. radius = 10 nm) can undergo rapid flocculation, which decreases the availability of active surface sites. Moreover, when the particle size decreases below a certain size, a quantization effect occurs, which causes the band gap to increase, leading to a decrease in photocatalytic activity [32]. Therefore, optimizing the particle size of photocatalysts is essential to improve their photocatalytic activity [32,35]. This result is consistent with the above computational results, showing that the most active photocatalyst in hydrogen production is Ga-M with particle size 28 nm. Related to this, it is possible to increase the thickness of the Ga oxide coverage layer above its native value in atmospheric conditions by utilizing higher electric fields and an oxidizing environment during the fabrication process [36]. In this way, it would be possible to achieve large metallic/semimetalic particles with a strong plasmonic enhancement of the electric field, and simultaneously with a thick oxide coverage ensuring a sufficient electron-hole pair generation.

6. Conclusions

In this work were presented the nanostructures Ga_2O_3/Ga/Graphene/SiO_2/Si prepared by method with controlled growth of the Ga islands, where the growth control was realized by varying the substrate temperature, which also affects the properties of these materials. With increasing substrate temperature, the ratio of nano-islands increased, but their number, surface area and also volume decreased as a consequence of the constant amount of deposited material. The thin surface ultra-wide band gap Ga_2O_3 effectively transforms incident electromagnetic wave energy into electron-hole pair production and the metallic Ga cores enhance the electric field separating charge carriers by the formation of localized surface plasmon resonances. Both these effects increase the amount of hydrogen yield during photocatalytic reaction. The most active photocatalyst was Ga-M, which not only produce high amounts of electron-hole pairs and separated them but also has optimal particle size (radius = 14 nm).

The studied materials are usually used in photodetectors, solar cells, and high-power electronics, but in this work, we have discovered new and very promising application in photocatalysis. A relatively small amount of these materials exhibited photocatalytic activity by successful hydrogen generation. The influence of Ga_2O_3/Ga/Graphene/SiO_2/Si on photocatalytic hydrogen generation has not been studied so far. When converted hydrogen yields to μmol/g according to the active material Ga_2O_3/Ga (2 μg), these investigated samples were found to have many times (in case of Ga-M >50 thousand times) higher activity than the commonly available commercial TiO_2. Another important advantage is that these samples can be reused without degradation, which was verified by reuse in the reaction (5 times); and removed from the reactor after the reaction without filtration or other methods for separation of photocatalyst from solution. The next direction of our research with this type of materials can be in other photocatalytic reactions (for example photocatalytic reduction of CO_2) and with using visible irradiation, but it will be possible with a bigger amount of samples.

The significance of our work lies in the fundamental research of a new system enabling the photocatalytic production of H_2 utilizing Ga

nanoparticles covered by a Ga_2O_3 thin layer on graphene. It can be treated as a general and modeling system, where a thin surface Ga_2O_3 layer is a source of electron-hole pairs suppressing typical bulk recombination, bulk Ga core plasmonically enhancing the electric field resulting in further increase of electron-hole pair creation efficacy, and graphene layer serving as a conductive support for efficient compensation of charge imbalance. In order to move toward more applied research, it would be necessary to reduce the energy consumption and costs of the fabrication process, which can be achieved by e. g. substituting the UHV technology with colloidal Ga NP preparation and substituting the CVD graphene by less demanding chemically-exfoliated graphene. The recent system involving Ga_2O_3 shell is also limited to UVC electromagnetic waves involved in sunlight in space, but not reaching the ground. Related to this, the Ga2O3 could be substituted by a semiconductor with a smaller energy band gap, e.g. GaN (3.4 eV), which can be produced by Ga NP nitridation.

CRediT authorship contribution statement

Miroslav Bartošík: Conceptualization, Formal analysis, Investigation, Methodology, Supervision, Writing – original draft. **Miroslava Filip Edelmannová:** Data curation, Investigation. **Jindřich Mach:** Data curation, Investigation. **Kamila Kočí:** Conceptualization, Formal analysis, Investigation, Methodology, Supervision, Writing – original draft and revised manuscript.

Declaration of competing interest

The authors declare that they have no known competing financial interests or personal relationships that could have appeared to influence the work reported in this paper.

Data availability

Data will be made available on request.

Acknowledgement

The work was supported from Large Research Infrastructure ENREGAT (project No. LM2023056).

References

[1] S.A. Younis, E. Amdeha, R.A. El-Salamony, Enhanced removal of p-nitrophenol by β-Ga_2O_3-TiO_2 photocatalyst immobilized onto rice straw-based SiO_2 via factorial optimization of the synergy between adsorption and photocatalysis, J. Environ. Chem. Eng. 9 (2021) 104619.
[2] N. Rungjaroentawon, S. Onsuratoom, S. Chavadej, Hydrogen production from water splitting under visible light irradiation using sensitized mesoporous-assembled TiO_2–SiO_2 mixed oxide photocatalysts, Int. J. Hydrog. Energy 37 (2012) 11061–11071.
[3] Q. Lu, L.-L. Zhang, T.-T. Xu, B.-Y. Zhang, W.-J. Gong, Highly efficient photocatalytic water splitting in direct Z-scheme α-In_2Se_3/are van der Waals heterostructures, Surfaces and Interfaces 36 (2023) 102608.
[4] M. Ge, C.-L. Yang, M.-S. Wang, X.-G. Ma, Photocatalytic hydrogen generation from overall water splitting with direct Z-scheme driven by two-dimensional InTe/Bismuthene heterostructure, Int. J. Hydrog. Energy 48 (2023) 138–146.
[5] F. Du, D. Yang, T. Kang, Y. Ren, P. Hu, J. Song, F. Teng, H. Fan, SiO_2/Ga_2O_3 nanocomposite for highly efficient selective removal of cationic organic pollutant via synergistic electrostatic adsorption and photocatalysis, Sep. Purif. Technol. 295 (2022) 121221.
[6] A. Vivian, L. Soumoy, L. Fusaro, P. Louette, A. Felten, S. Fiorilli, D.P. Debecker, C. Aprile, The high activity of mesoporous Ga-SiO_2 catalysts in the upgrading of glycerol to solketal explained by in-depth characterization, J. Catal. 400 (2021) 83–92.
[7] D.L. Staebler, C.R. Wronski, Optically induced conductivity changes in discharge-produced hydrogenated amorphous silicon, J. Appl. Phys. 51 (1980) 3262–3268.
[8] I.S. Altman, D. Lee, J.D. Chung, J. Song, M. Choi, Light absorption of silica nanoparticles, Phys. Rev. B 63 (2001) 161402.
[9] M. Kobayashi, F. Juillerat, P. Galletto, P. Bowen, M. Borkovec, Aggregation and charging of colloidal silica particles: effect of particle size, Langmuir 21 (2005) 5761–5769.
[10] J. Mach, P. Procházka, M. Bartošík, D. Nezval, J. Piastek, J. Hulva, V. Švarc, M. Konečný, L. Kormoš, T. Šikola, Electronic transport properties of graphene doped by gallium, Nanotechnology 28 (2017) 415203.
[11] D. Nezval, M. Bartošík, J. Mach, J. Piastek, V. Švarc, M. Konečný, T. Šikola, Density functional study of gallium clusters on graphene: electronic doping and diffusion, J. Phys. Condens. Matter 33 (2021) 025002.
[12] A. Tayel, A.R. Ramadan, O.A. El Seoud, Titanium Dioxide/Graphene and Titanium Dioxide/Graphene Oxide Nanocomposites: Synthesis, Characterization and Photocatalytic Applications for Water Decontamination, Catalysts, 2018.
[13] V. Singh, D. Joung, L. Zhai, S. Das, S.I. Khondaker, S. Seal, Graphene based materials: past, present and future, Prog. Mater. Sci. 56 (2011) 1178–1271.
[14] A.K. Geim, K.S. Novoselov, The rise of graphene, Nat. Mater. 6 (2007) 183–191.
[15] C. Yi, T.-H. Kim, W. Jiao, Y. Yang, A. Lazarides, K. Hingerl, G. Bruno, A. Brown, M. Losurdo, Evidence of Plasmonic coupling in gallium nanoparticles/graphene/SiC, Small 8 (2012) 2721–2730.
[16] M.J. Hernández, M. Cervera, E. Ruiz, J.L. Pau, J. Piqueras, M. Avella, J. Jiménez, Gallium-assisted growth of silicon nanowires by electron cyclotron resonance plasmas, Nanotechnology 21 (2010) 455602.
[17] M. Zhu, P. Chen, M. Liu, Ag/AgBr/graphene oxide nanocomposite synthesized via oil/water and water/oil microemulsions: a comparison of sunlight energized Plasmonic photocatalytic activity, Langmuir 28 (2012) 3385–3390.
[18] M. Zhu, P. Chen, M. Liu, Graphene oxide enwrapped ag/AgX (X = Br, cl) nanocomposite as a highly efficient visible-light Plasmonic Photocatalyst, ACS Nano 5 (2011) 4529–4536.
[19] Y. Wen, H. Ding, Y. Shan, Preparation and visible light photocatalytic activity of ag/TiO_2/graphene nanocomposite, Nanoscale 3 (2011) 4411–4417.
[20] M.W. Knight, T. Coenen, Y. Yang, B.J.M. Brenny, M. Losurdo, A.S. Brown, H. O. Everitt, A. Polman, Gallium Plasmonics: deep subwavelength spectroscopic imaging of single and interacting gallium nanoparticles, ACS Nano 9 (2015) 2049–2060.
[21] J. Čechal, T. Matlocha, J. Polčák, M. Kolíbal, O. Tomanec, R. Kalousek, P. Dub, T. Šikola, Characterization of oxidized gallium droplets on silicon surface: an ellipsoidal droplet shape model for angle resolved X-ray photoelectron spectroscopy analysis, Thin Solid Films 517 (2009) 1928–1934.
[22] S.J. Pearton, J. Yang, P.H. Cary, F. Ren, J. Kim, M.J. Tadjer, M.A. Mastro, A review of Ga_2O_3 materials, processing, and devices, Appl. Phys. Rev. 5 (2018) 011301.
[23] K. Kočí, I. Troppová, M. Edelmannová, J. Starostka, L. Matějová, J. Lang, M. Reli, H. Drobná, A. Rokicińska, P. Kuśtrowski, L. Čapek, Photocatalytic decomposition of methanol over La/TiO^2 materials, Environ. Sci. Pollut. Res. Int. 25 (2018) 34818–34825.
[24] S.A. Maier, Plasmonics, Springer, New York, 2007.
[25] M. Fox, Optical Properties of Solids / Mark Fox, Second edition. ed, Oxford University Press, Oxford [U.K.], 2010.
[26] S. COMSOL Multiphysics® v. 6.1. www.comsol.com. COMSOL AB, Sweden.
[27] S. Rafique, L. Han, H. Zhao, (invited) Ultrawide bandgap β-Ga_2O_3 thin films: growths, Properties and Devices, ECS Transactions 80 (2017) 203.
[28] X. Zhang, Z. Zhang, J. Liang, Y. Zhou, Y. Tong, Y. Wang, X. Wang, Freestanding single layers of non-layered material γ-Ga_2O_3 as an efficient photocatalyst for overall water splitting, J. Mater. Chem. A 5 (2017) 9702–9708.
[29] H. Ryou, T.H. Yoo, Y. Yoon, I.G. Lee, M. Shin, J. Cho, B.J. Cho, W.S. Hwang, Hydrothermal synthesis and photocatalytic property of Sn-doped β-Ga_2O_3 nanostructure, ECS J. Solid State Sci. Technol. 9 (2020) 045009.
[30] L. Yuliati, T. Hattori, H. Itoh, H. Yoshida, Photocatalytic nonoxidative coupling of methane on gallium oxide and silica-supported gallium oxide, J. Catal. 257 (2008) 396–402.
[31] S.H. Mohamed, M. El-Hagary, S. Althoyaib, Growth of β-Ga_2O_3 nanowires and their photocatalytic and optical properties using Pt as a catalyst, J. Alloys Compd. 537 (2012) 291–296.
[32] K. Kočí, L. Obalová, L. Matějová, D. Plachá, Z. Lacný, J. Jirkovský, O. Šolcová, Effect of TiO_2 particle size on the photocatalytic reduction of CO_2, Appl Catal B 89 (2009) 494–502.
[33] M. Murdoch, G.I. Waterhouse, M.A. Nadeem, J.B. Metson, M.A. Keane, R.F. Howe, J. Llorca, H. Idriss, The effect of gold loading and particle size on photocatalytic hydrogen production from ethanol over au/TiO_2 nanoparticles, Nat. Chem. 3 (2011) 489–492.
[34] H. Yin, T. Tsuzuki, K.R. Millington, P.S. Casey, A comparative interlaboratory study on photocatalytic activity of commercial ZnO and CeO_2 nanoparticles, J. Nanopart. Res. 16 (2014).
[35] S. Chen, H. Yin, P. Liu, Y. Wang, H. Zhao, Stabilization and performance enhancement strategies for halide perovskite Photocatalysts, Adv. Mater. 35 (2023) e2203836.
[36] M. Bartošík, D. Skoda, O. Tomanec, R. Kalousek, P. Jánský, J. Zlámal, J. Spousta, T. Sikola, The influence of humidity on the kinetics of local anodic oxidation, J. Phys. Conf. Ser. 61 (2007) 75.